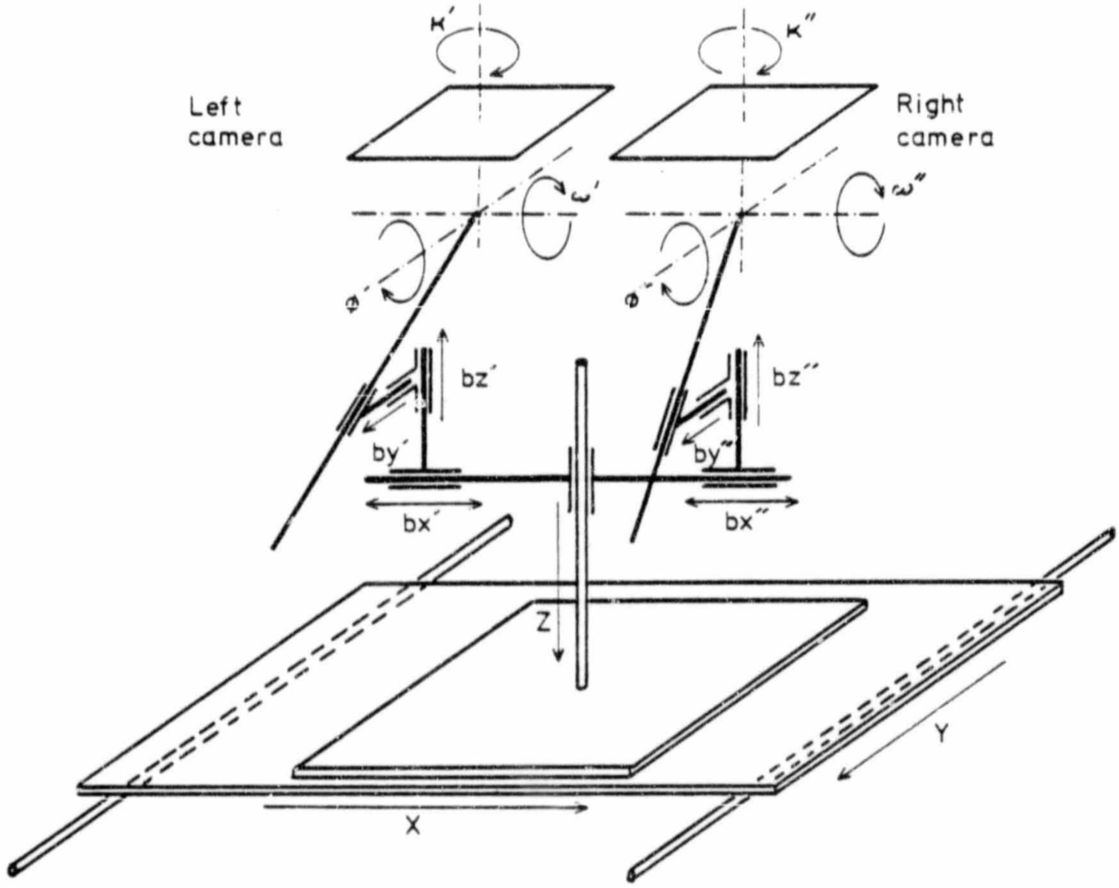

FIGURE A.1 Sketch illustrating the mechanical arrangements of the Wild A7 Autograph.

FIGURE A.2 Sketch illustrating how the control points on the reference grid were co-ordinated in the Wild A7 Autograph.

recorded in A7 plotter units. The first two photographs of both the static and dynamic tests were measured in some detail. Analysis of this data showed that measureable displacements could not be detected throughout the area of the reference grid and the number of squares measured in subsequent photographs was consequently reduced to 36.

Once the initial pair of photographs had been measured, the first photograph was removed from the left plotting camera and the third photograph, again suitably aligned on the picture carrrier, was put into its place. The co-ordinate measurement procedure was then repeated but this time data was collected for the photograph in the left camera only. The next photograph was then placed in the right hand camera, and so on until the end of the sequence.

Actual grain displacements were obtained from the co-ordinate data gathered in this manner by subtracting the co-ordinates of the sand grains measured in the first photograph from the co-ordinates of the same grains measured in subsequent photographs. The displacements were thus obtained in terms of X and Y components. However, because the control points in any pair of photographs were not always necessarily aligned in precisely similar positions on the stereoplotter picture carriers, and because of the possibility of image distortions (discussed in section A.3), the co-ordinate data measured on photographs taken after the first photograph, had to be transformed to equivalent positions on the first photograph. The procedure used to perform this transformation is discussed in section A.2.

A.2 Co-ordinate Transformation

Figure A3 illustrates how light rays projected through the camera lens from a portion of the face of the sand box would form an image of a group of four control points on both a correctly aligned and a misaligned photograph. Figure A4 shows where the images of these control points would have appeared in the stereo-plotter with respect to their common co-ordinate system. It is clear that the quadrilateral defined by the control points on the misaligned photograph is both deformed relative to the shape defined by the same control points on the correctly aligned photograph, as well as laterally displaced. In order to obtain data on the displacements of the sand grains to an accuracy limited mainly by measurment error, a procedure was required to transform the co-ordinates of points measured on a misaligned photograph, into equivalent points on the first and correctly aligned photograph. The procedure used to perform the necessary transformations was kindly developed for this project by Professor J.M. Ridley and Dr G.S. Wells of the Mathematics Department at the

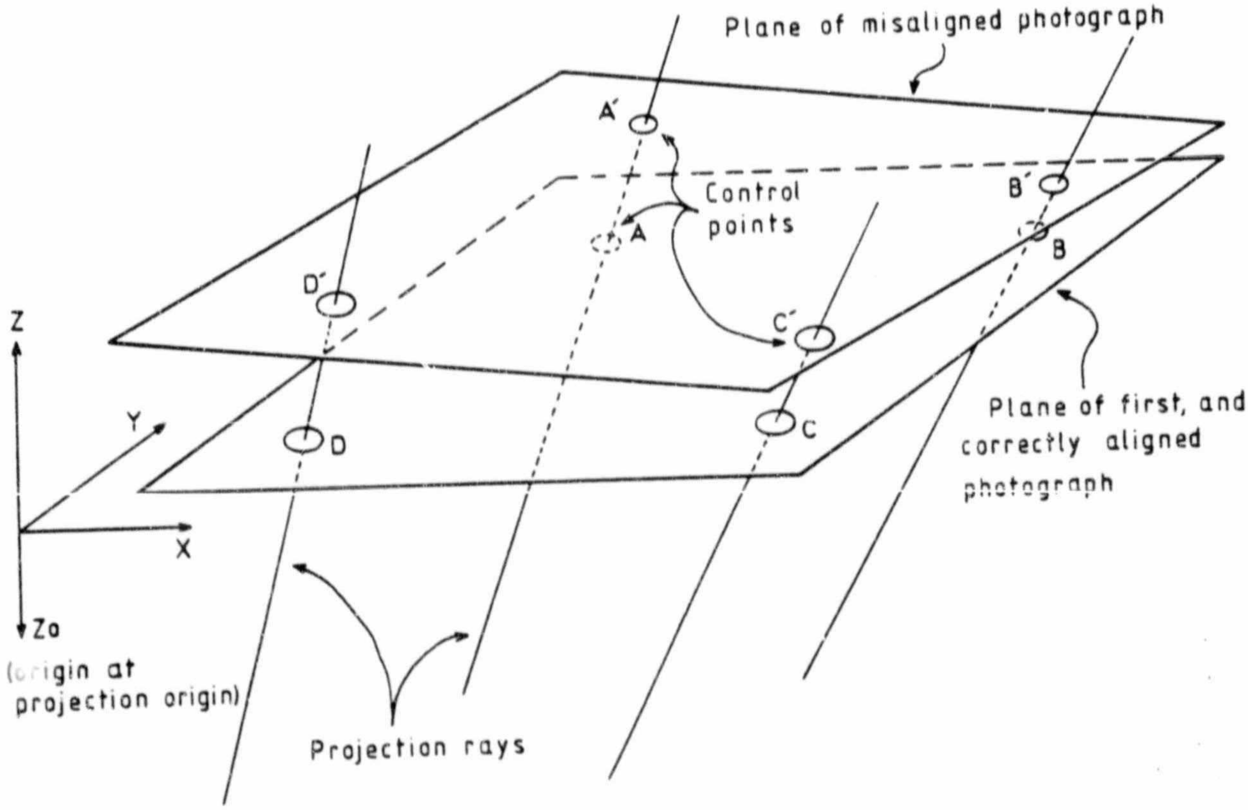

FIGURE A.3 Geometrical relationships between control points located on correctly aligned and misaligned photographs.

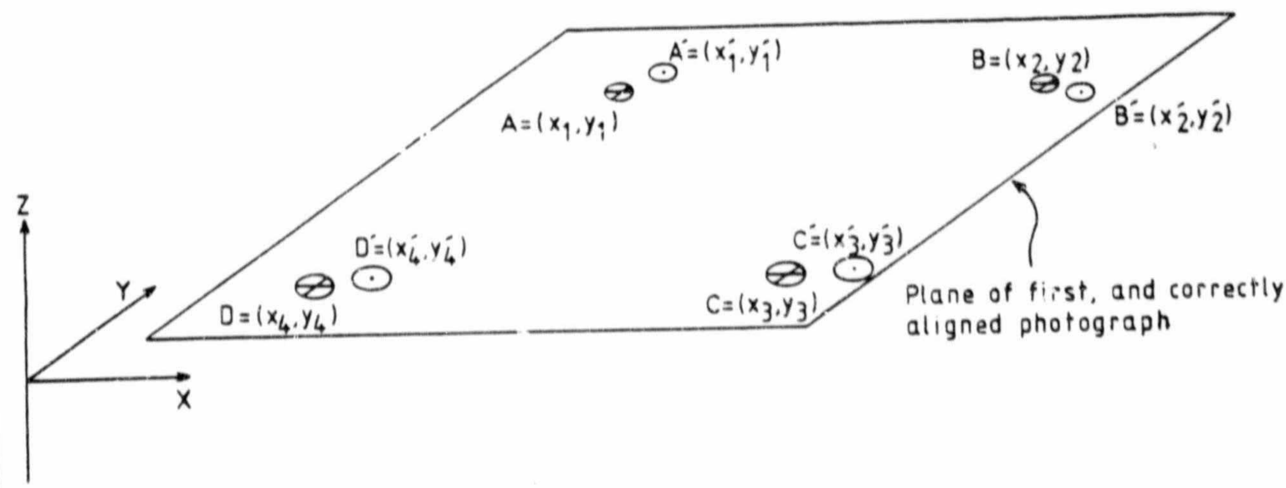

FIGURE A.4 Illustrates the positions of control points on a misaligned photograph superimposed on a correctly aligned photograph.

University of the Witwatersrand. (The writer, however, assumes sole responsibility for application of the method to this project and for interpretation of the results.)

The method, which is based on principles of projective geometry, treats each co-ordinate pair as a vector. It is described here without proof. A computer programme was written to perform the calculations. In the programme, co-ordinate data for a group of four control points in the first and subsequent photographs was used to solve for a set of transformation coefficients (referred to as the A matrix). These coefficients were then applied to the co-ordinates of sand grains located within that group of control points on the misaligned photographs to obtain corrected co-ordinates with which the grain displacements were calculated. The programme then repeated this process on another group of four control points until all the measured data had been analysed. It is considered that by applying co-ordinate transformations to localised and small regions of the displacement photographs, the majority of the errors affecting the accuracy of the calculated displacements (discussed in section A.3), were kept small.

Referring to Figure A4, the co-ordinates of the control points on the misaligned photograph may be described as defining four "incorrect" prints corresponding to four "correct" points on the correctly aligned photograph.

Correct Points			Incorrect Points			
A	=	(x1, y1)	A'	=	(x1', y1')	
B	=	(x2, y2)	B'	=	(x2', y2')	(A-1)
C	=	(x3, y3)	C'	=	(x3', y3')	
D	=	(x4, y4)	D'	=	(x4', y4')	

Using this data two matrices can be formed:

$$X = \begin{bmatrix} x1 & x2 & x3 \\ y1 & y2 & y3 \\ c & c & c \end{bmatrix} \quad \text{and} \quad X' = \begin{bmatrix} x1' & x2' & x3' \\ y1' & y2' & y3' \\ c & c & c \end{bmatrix} \quad (A-2)$$

The item 'c' in these matrices may be thought of as describing the height of the photographs above the projection ori..n at the time the exposures were made. The numerical value chosen for 'c' is theoretically not important, however, provided it is not equal to 0. Limitations to the range of numbers which could be adequately manipulated by the computer used for this project, however, required that 'c' be given a value which was of a similar order of magnitude as the co-ordinate data. Because X and Y co-ordinate values ranged from about 8 000 to 200 000, 'c' was assigned a value of 100 000.

After inverting the X and X' matrices, two column vectors can be formed from the product of the inverted matrices and the co-ordinates of the fourth control point.

$$\begin{bmatrix} u1 \\ u2 \\ u3 \end{bmatrix} = X^{-1} \begin{bmatrix} x4 \\ y4 \\ c \end{bmatrix} \quad \text{and} \quad \begin{bmatrix} u1' \\ u2' \\ u3' \end{bmatrix} = (X')^{-1} \begin{bmatrix} x'4 \\ y'4 \\ c \end{bmatrix} \qquad \text{(A-3)}$$

These can then be used to generate a diagonal matrix:

$$D = \begin{bmatrix} u1/u1' & 0 & 0 \\ 0 & u2/u2' & 0 \\ 0 & 0 & u3/u3' \end{bmatrix} \qquad \text{(A-4)}$$

The matrix containing the required transformation co-efficients, the A matrix, may then be obtained by the matrix multiplication:

$$A = X.D.(X')^{-1} \qquad \text{(A-5)}$$

Then, for any co-ordinated point (x', y') such as a sand grain, on the misaligned photograph, a column vector can be obtained by finding the product:

$$\begin{bmatrix} r \\ s \\ t \end{bmatrix} = A \begin{bmatrix} x' \\ y' \\ c \end{bmatrix} \qquad \text{(A-6)}$$

We define,

$$t' = t/c \qquad \text{(A-7)}$$

The equivalent point (x", y") on the correctly aligned photograph is then found as:

$$(x'', y'') = (r/t', s/t') \qquad \text{(A-8)}$$

The procedure described was tested in a number of ways and found to be numerically precise. In particular, checks on the precision with which the co-ordinates of the "incorrect" control points were transformed to the "correct" control points indicated that the resulting numerical error was in general significantly less than 1 co-ordinate unit. This precision is well in excess of the range of possible measurement errors which are discussed in section A.3.

A.3 Data Accuracy

The magnitude of the displacement components of moving sand grains determined by using the methods described, was subject to a number of potential sources of error. Some of these potential sources of error are common to any photographic method of determining planar displacement fields, while others are unique to the equipment used in this project. It is suggested that, in general, the uncertainty with which the co-ordinates of the sand grains were measured was significantly greater than the magnitude of the uncertainty due to other causes. The scale of the sand displacement photographs, which is typically limited by practical considerations, was therefore of primary importance. Some causes of experimental uncertainty influencing the calculated sand grain displacements are discussed below. (See also Andrawes [1976].)

(i) Camera lens distortion: Superior quality lenses such as those used in photogrammetric work are specifically manufactured to minimise distortion of the image. Less sophisticated lenses, such as that used in this project, while providing sharp focus and crisp images, may project a distorted image. Because the observed soil movements were small in relation to the overall size of the image produced by the lens, individual sand grains monitored during a sequence of exposures were generally located in close proximity to one another. They were therefore subjected to approximately similar amounts of distortion. Consequently, although the true position of the sand grains may not have been measured, the error in the relative positions as determined in a sequence of exposures, and therefore the error in the measured grain displacements, would have been small. In view of this reasoning, the magnitude of errors due to camera lens distortion has not been investigated, but it is considered that they will have been significantly less than measurement errors.

(ii) Distortion of the reference grid control points could have occurred during a sequence of exposures. Changes in humidity and temperature around the test rig could have caused random dimensional changes amongst the paper discs used as control points on the glass face of the sand box. Under the essentially constant ambient laboratory conditions which existed during the pile testing, it is considered that errors from these sources may be neglected.

As the model pile was driven or pushed downwards against the glass face of the sand box, a horizontal component of force was developed by movement of the soil past the cone shaped shoe. During development of the model pile test rig and test procedures, measurements of the outward deflection of the glass panel caused by this horizontal load component, were obtained during impact installation. Dial gauges, placed along the centre line (corresponding to the pile axis) of the outer face of the glass panel at depth of 395mm and 745mm recorded a progressive increase in horizontal deflections of at most 0,42mm from the initial at rest position as the pile was driven past the gauge. The greatest deflections occurred shortly after the top of the pile shoe passed below the dial gauge. Deflections between impacts ranged from 0,01mm to 0,05mm as the pile neared the gauge. No similar deflection measurements were carried out during static load tests. It is suggested that as a result of impact installation the glass wall was effectively preloaded and therefore deflected to an equilibrium condition compatible with the horizontal forces which could have developed during the static load tests. Deflection during these tests was therefore probably significantly less than 0,42mm. Deflection of the glass panel on which the control points were attached induces errors of three kinds.

If it is assumed that the deflected shape of the glass panel can be approximated by a segment of a parabola where the distance between the mid-point of a chord representing the undeflected glass face and the extremity of the parabola is 0,42mm, then, for the dimensions of sand box used, the extension of the outer fibre of the parabola can be calculated as $3,9 \times 10^{-4}$mm (see Figure A.5). A distortion of this magnitude spanning the control points was less than the resolution of the equipment used in co-ordinating the photographs.

Horizontal deflection at the mid-point of the glass panel may also be considered as approximately equivalent to an induced rotation of the panel containing the control points about a hinge located at the edge of the sand box (see Figure A.6). Assuming a rotation of 0,42mm and applying it to the dimensions of the sand box and camera system, it can be shown that the image obtained of the rotated plane would over-estimate the width spanned by the control points by about 0,1mm (an error 0,03%). Consequently co-ordinates of control points measured on the photographs would not correctly correspond to the co-ordinates of the same points if they were measured on the glass panel. Once again, however, true co-ordinate values were less important than the relative values in a sequence of photographs. Because displacements were small and all co-ordinate data was transformed to equivalent data in the first exposure, the error in the calculation of the displacements of the sand grains would be small. Again, because the glass panel would have been curved (approximately as shown in Figure A.5), the percentage error at each point would have been less than the percentage error determined across the width of the control points. Errors due to horizontal deflection of the glass front of the sand box to which the control points were attached are therefore considered negligible.

Outward movement of the glass plate in the vicinity of the pile shoe disturbs the structure of the initially homogenous soil and could result in a density reduction in a zone bordering the surface on which the soil displacements are measured. It would also interfere with the assumed axisymmetric behaviour of the model pile, particularly by permitting asymmetric circumferential soil movements. Arthur and Roscoe (1965) have shown that side plate deflection in model retaining wall experiments can have a profound influence on the measured wall force at outward wall deflections of as little as 0,15mm.

Whilst both loads and grain displacements measured during this model pile testing programme will undoubtedly have been affected by this form of "edge effect", it is suggested that the influence on the data will be less profound than that observed by Arthur and Roscoe (op cit). Reasons for this opinion may be summarised as follows.

The plate deflection was measured in a position where the maximum deflection could be expected at a point furthermost from supports. This is the zone of greatest soil movements. Smaller soil movements occurred nearer to positions of zero deflection of the glass. Soil movements were recorded to about 3,2 pile diameters below the pile shoe and to about 3,6 pile diameters to the side of the pile. Within this region, the soil was subjected to considerable and progressive remoulding with each successive impact leading to significant densification of the soil towards the pile shoe. Although the nett wall plate deflection was measured as 0,42mm, between individual impacts the deflections were of the order of 0,03mm. It is suggested that the accumulated effect of remoulding the soil during each impact, associated with small individual plate deflections, would contribute greatly towards ensuring that the assumed axisymmetric condition is a reasonable approximation.

(iii) Plate film distortions: Plate film used for aerial photogrammetric survey work is often supplied in the form of a photographic emulsion applied to a glass sheet which is both dimensionally stable and plane. Alternatively, when roll film of the type used for this project is used in aerial surveys, the film is placed inside the camera against a precisely planed and aligned perforated plate connected to a low vacuum. The vacuum holds the film against the plate via the perforations ensuring that the film is [illegible] in position and held plane during

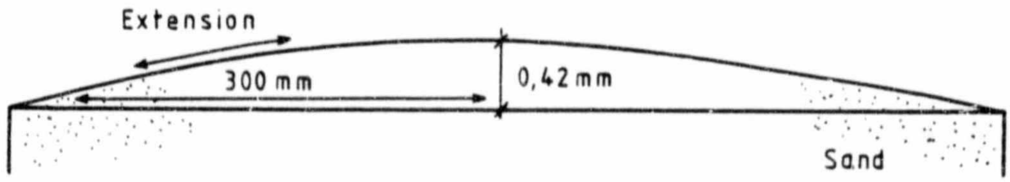

FIGURE A.5 Parabolic deflection of the glass plate.

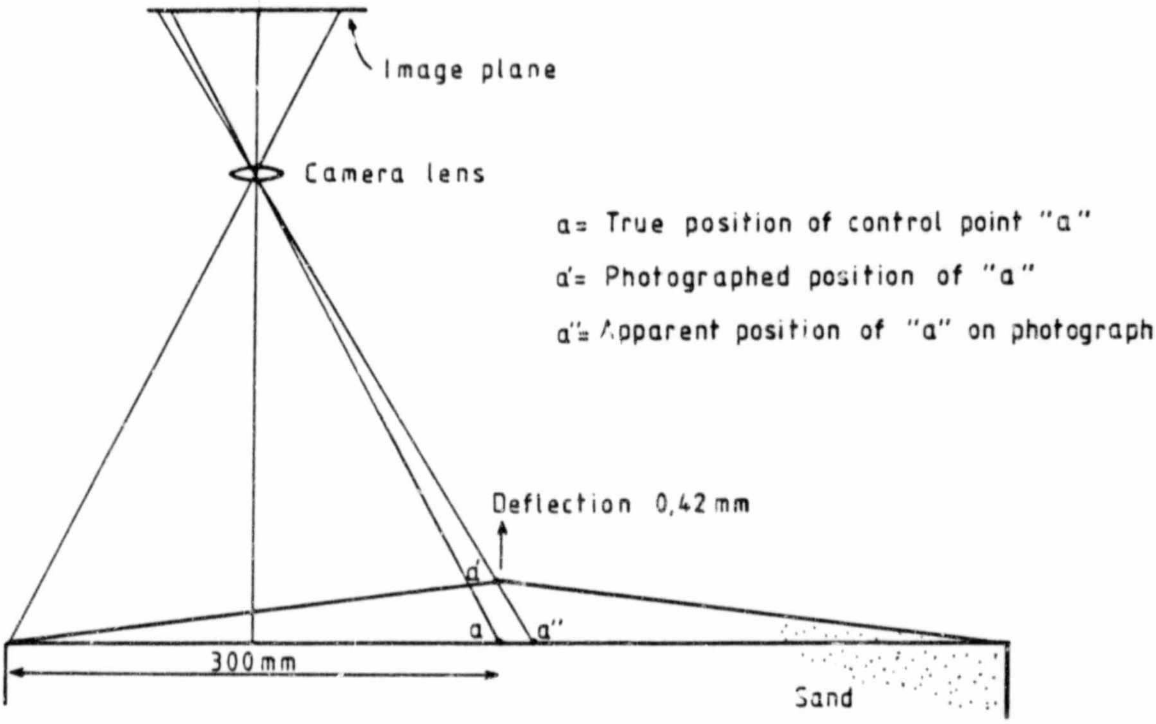

FIGURE A.6 Deflection of the glass plate approximated as a rotated plane.

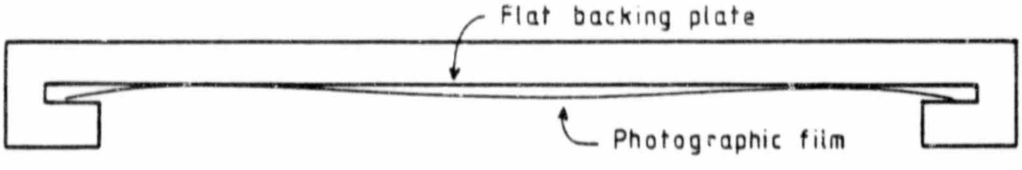

FIGURE A.7 Section through film holder showing possible distortion of a sheet of photographic film.

NOTE: These diagrams are not drawn to scale.

exposure. Vacuum equipment was not used during exposure of the soil displacement photographs for this project, and it is likely that in most cases the image plane was not entirely flat. The errors caused by the sheet film not being flat are of a similar type to those discussed in (ii) above. Distortion of the sheet film was kept to a minimum, however, by exploiting the natural curvature of the film, concave on the emulsion side, in the design of the film holders (see Figure A.7). Errors in the estimation of the sand grain displacements caused by the sheet film not being flat, are similar to those discussed in (ii), and may be neglected for similar reasons.

Changes in the dimensions of the photographs due to temperature and humidity changes were not investigated. Because ambient conditions during exposure, development and measurement of the photographs were the same for any particular group of photographs, the photographs would have been subjected to similar distortions. Errors caused by changes in the photograph dimensions are therefore considered to be small.

(iv) Due to the nature of the camera equipment used, it was possible for the alignment of the image plane to change during a sequence of exposures.

The possible movements and resulting distortions are shown diagrammatically in Figures A.8a and A.8b. Removal of errors due to image plane misalignment has been discussed in section A.2.

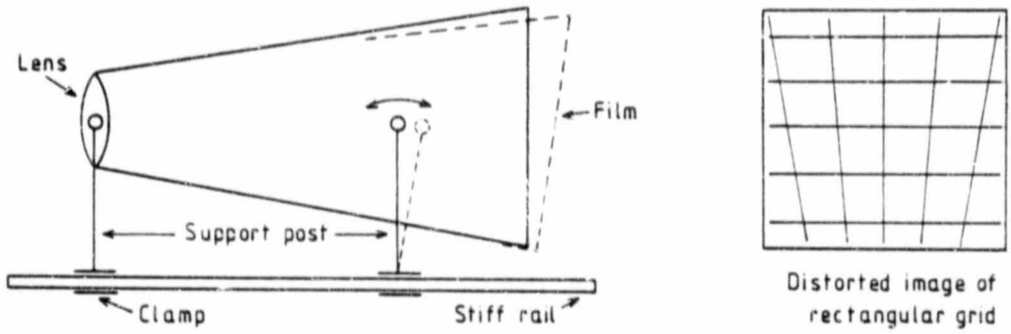

Figure A.8a

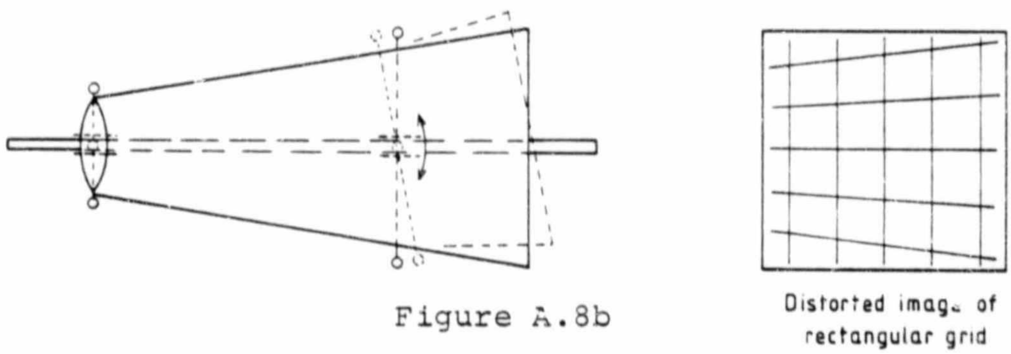

Figure A.8b

Figure A.8a — Side elevation of camera showing possible rotation of camera support post about horizontal axis and resulting image distortion.

Figure A.8b — Plan view of camera showing possible rotation of camera image plane about a vertical axis and resulting image distortion.

Note: Rotations greatly exaggerated.

Figure A.8 — Effect of image plane rotations.

(v) Measurement accuracy. The precision and accuracy, or degree of uncertainty, with which co-ordinate measurements were made in the Wild A7 Autograph, was influenced by accuracy limitations of the stereoplotter itself as well as by difficulties experienced in placing the stereoplotter's measuring mark on a point to be co-ordinated.

Calibration measurements carried out on the Wild A7 Autograph used for this [illegible]ject indicated that the equipment was accur[illegible] a 200mm span to ± 0,0017mm at 95% confiden[illegible]its. This may be considered a fixed error applicable to all the stereoplotter measurements. At the scale of the model pile, the equivalent measurement error range was ±0,0029mm. The sand grain displacement contour diagrams (Figures 5.2 to 5.5, and 5.10 to 5.17) have been drawn using stereoplotter units as the measure of displacement, where 1 plotter unit = 0,00118mm. Limitations in the accuracy of the equipment therefore restricts the accuracy of the contour values to a range of approximately ± 3,5 contour units.

Of significantly greater influence on the accuracy with which points on the photographs were co-ordinated, however, was the precision with which the selected points could be measured.

All the control points were routinely measured at least 3 times, and most measurements were repeated 6 or 12 times. A considerable amount of data was therefore available for statistical analysis. Similar data was collected by repeating co-ordinate measurements 10 times, on each of 20 randomly selected sand grains in one of the photographs. Table A.3.1 presents the results of an analysis, assuming that the errors were random and followed Gaussion distribution, of the data gathered from two photographs for 117 control points and for the 20 sand grains.

Table A.3.1 : A summary of measurement data accuracy for both control points and sand grains

Statistical check	Control Points Plotter Units	Sand Grains Plotter Units
Average of the range of measured X co-ordinates	14	17
Maximum range of measured X co-ordinates	48	53
Average of standard deviations, X co-ordinates	5,5	7
95% confidence limits, X co-ordinates	± 6	± 7,5
Average of the range of measured Y co-ordinates	10	14
Maximum range of measured Y co-ordinates	34	46
Average of standard deviations, Y co-ordinates	4,5	6
95% confidence limits, Y co-ordinates	± 5	± 6

It is not certain why measurement of the Y axis co-ordinate data was more precise than the X axis data. This feature may be related to the way in which the points were co-ordinated. When placing the measuring mark in the stereoplotter onto a point to be co-ordinated, the routine practise was to locate the mark by first applying Y carriage movements. This was done by tracking back and forth across the point until coincidence of the measuring mark and the co-ordinate point was satisfactorily achieved in the Y axis direction. Final positioning of the measuring mark was made by applying a single X carriage movement. Effectively, therefore, many more Y axis than X axis measurements were made for each pair of co-ordinate values obtained.

Because data in a pair of photographs were compared in order to otained sand grain displacements, the errors given in Table A1.1 are cumulative. Also, because sand grain co-ordinates were obtained with respect to the control points in the co-ordinate transformation process, their error must be added to the sum of the control point errors. The fixed error, due to equipment limitations, is incorporated in the measurement errors. If it is accepted that the statistical data presented for both the 117 control points and the 20 sand grains are representative of all the measurements made of the two types of co-ordinated points, and that errors due to previously discussed sources may be neglected, it may be concluded that within 95% confidence limits, the individual sand grain displacements were determined with the following uncertainties:

X displacements ± 27 plotter units (= ± 0,032mm)
Y displacements ± 22 plotter units (= ± 0,026mm)

These errors are of a similar order of magnitude as those found by, for example, Luker (1984) when using stereo-superposition of photo pairs. Thus, "Published case histories and my own experience show that an accuracy of 0,02mm of relative movement on the film can easily be achieved with an ordinary camera and a good quality stereo-plotter with an inexperienced operator". (Luker, [1984, p.376]). For this project, 0,02mm relative movement on the film corresponded to 0,036mm on the scale of the model pile.

(vi) Edge effects at the glass wall/soil interface: Arthur and Roscoe (1965) investigated how interface friction between a glass wall and a contained sand affected the soil displacements observed to occur at the edge of and within a plane strain model retaining wall experiment. They concluded that the interface friction was small and induced errors of no more than 10% in calculated shear strains. They do, however, suggest that the influence of wall friction should be investigated for particular applications. Butterfield (1977, private communication to Dr I. Luker, University of the Witwatersrand) reported that, in footing experiments, the restriction of the displacement field by glass friction was found to be much less than the repeatability of nominally identical experiments.

It is suggested that interface friction is unlikely to have a major influence on the accuracy of the displacement data presented for this project.

A.4 Accuracy of Displacement Contour Diagrams

The accuracy of the grain displacement diagrams needs to be considered from two aspects. Firstly, are the contour lines drawn in the correct position and, secondly, what is the uncertainty field associated with these positions?

The grain displacement contour diagrams (Figures 5.2 to 5.5 and 5.10 to 5.17) were drawn by visually interpolating the calculated displacement data plotted by computer onto drawings which were about 4.5 x true scale. This data comprised at least 15 sand grains located within each approximately 30mm to a side quadrilateral, defined by each group of four control points. The interpolation process therefore relied on data points located at an average spacing of, at most, 8mm. Visual interpolation, although subjective, has an automatic data averaging and curve smoothing function. When applied to the drawing of contours, it can provide an efficient means of combining the available information to optimise the location of a contour line.

Whilst additional data points would probably have contributed to ensuring greater confidence in the plotted position of the displacement contours, it is considered that sufficient data was collected to enable the drawing of most of the contours to an accuracy limited mainly by measurement errors. It is suggested therefore that the contours reasonably represent the loci of most of the sand grains which were subjected to the same movement components, and that they are located within the uncertainty fields associated with measurement errors.

It has been shown that due mainly to measurement errors, the resolution to which the displacements of individual sand grains could be calculated was of the order of $\pm$ 25 plotter units at 95% confidence limits. Errors in the calculated displacements may be visualised on the grain displacement contour diagrams as an uncertainty field bounding the given position of any particular contour line. Where displacements were high, the plan width of this uncertainty field would be narrow, while in regions of small displacements, the uncertainty field would be wide. Consequently, the plan positions of contours indicating large movements may be accepted as given. The plan positions of contours indicating small movements must, however, be considered best estimates. In view of the comments made previously, it is suggested that "large" movements refer to displacements of 50 and above plotter units, and "small" movements refer to displacements of less than 50 plotter units.

In areas where the magnitude of the sand grain displacements varied considerably over a small distance, i.e. where contour lines converge, a relatively greater number of sand grains should ideally have been co-ordinated in order to minimise the use of interpolation. The technique described here, however, because it relies on identifying scattered clearly defined individual sand grains, made it impossible to co-ordinate a sufficient number of sand grains in some areas. Extensive interpolation was therefore applied in areas of high displacement gradients which generally comprised the boundary zones between pile and soil. Again, in order to preserve clarity in the presentation of the data, and prevent detail from obscuring the general trends, contours in areas of high displacement gradients have not always been shown in full. This is especially important along the margins to the face of the conical pile shoe where contours of the movements of sand grains lying initially in contact with the pile shoe are not shown. Indeed, nor were the movements of any such grains actually measured, mainly because suitable particles could not be identified in the photographs. Similar comments also apply to the contact zone along the pile shaft.

Theoretically, in Figures 5.10 to 5.17 which include elastic deformation of the soil, the boundary of the displacement field, and therefore the zero displacement contour, should lie at the edges of the sand container. Zero displacements contours lying well within this artificial boundary have, however, been drawn in all the displacement diagrams. They represent the limits of detectable soil movements and may be described as lines connecting areas in which grain displacements appeared to be random in either X or Y directions. In Figure A.9, the logarithm of the magnitude of the displacements has been plotted against distance from the pile shoe for Figures 5.2 and 5.4. If it is accepted that the straight line extrapolation shown on these graphs is meaningful it appears that, for these two drawings at least, the zero displacement boundary contour more correctly corresponds to the locus of X displacements of about 20 plotter units. It is suggested that in general the zero displacement boundary contours may be assumed to locate displacements of the order of 15 to 20 plotter units. Where this boundary separates fields of movement in opposite directions however, it correctly describes, in terms of the movement components plotted, the locus of points with zero relative displacement.

As a final comment, it must be noted that the drawing of the displacement contours using visual interpolation, may constitute a major weakness in this method of determining the displacements of the soil around the model pile. Up to the stage where the contours were drawn, all the data used was factual within calculable error ranges. The contouring process, however, imposed individual human bias to the data which will differ with different workers.

A.5 Axial Symmetry in the Model System

In the model system described in this report, the plane of the glass face panel theoretically lies precisely in a plane of symmetry located along the axis of the model pile. Also, all observed soil movements are theoretically those which would occur around a circular pile installed into a mass of soil sufficiently far from a rigid boundary such that no edge effects would disturb

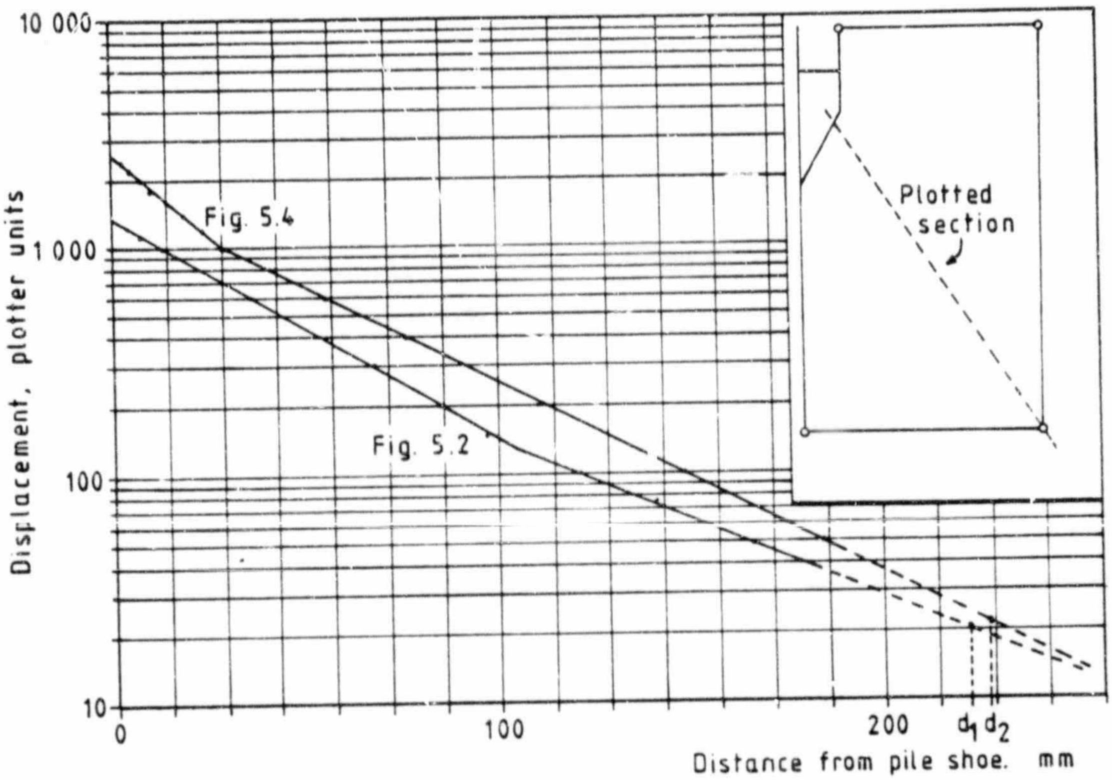

Figure A.9 Graph showing the logarithm of the displacements plotted against distance from the pile shoe for Figures 5.2 and 5.4 along the section shown. d1 and d2 show the positions of the plotted zero displacement contour on these figures.

the normal behaviour of the pile/soil system. Some edge effects have already been discussed, and it has been suggested that they may be considered to have a negligible influence on the significance of the measured sand grain displacements. Over most of the length of the pile it is considered that conditions of axisymmetry are adequately represented. Near the point of the pile toe, however, the experimental data suggest that symmetry conditions may not be maintained.

The inner face of the glass panel represents the theoretical plane of symmetry. Theoretically a significant number of sand grains should be cut by this plane, whereas in reality all the grains lie entirely to one side of it and will behave accordingly. The displacement patterns observed, therefore, apply to an approximate equivalent plane of symmetry lying about half of the average grain diameter back from the true plane of symmetry. The radius of curvature of the conical pile shoe increases towards the point, eventually becoming of a similar order of magnitude to the diameter of the sand grains themselves. Where the pile dimensions are not greatly different from the dimensions of the sand particles themselves, it seems inevitable that local effects, dependent on such factors as the shape of individual sand grains and the presence of surface asperities on the pile shoe, become important. Sand movements on the theoretical plane of symmetry then become 3-dimensional and axial symmetry is destroyed.

From the discussion in Chapter 6, section 6.2, it appears that such local effects are important near the point of the pile shoe over a zone from the point to where the radius of the cone is about 10 x the average diameter of the sand grains. This corresponds approximately to the bottom 16mm of the shoe cone, or about one third of the length of the inclined face of the cone. This phenomenon would not be a problem in a plane strain simulation with a wedge shaped shoe.

APPENDIX B

B.1 Dimensional Analysis

The selection of an adequate model system for the driven displacement grouted in-situ MV piles requires consideration of both the pile dynamics during installation and the pile/soil interaction under static loading conditions.

B.1.1 Dynamic Analysis

The similitude requirements of the model pile during dynamic loading were investigated using a dimensional analysis of moving rigid bodies impacting on geometrically similar systems presented by Langhaar (1951, p.94). Langhaar (op.cit) concludes from the analysis that, "... the model and prototype experience the same stresses when they are struck by bodies moving with the same speed ... provided that the masses of the incident bodies are proportional to the cubes of the linear dimensions of the structures."

The linear scaling for the model pile used for this project was approximately 1/6 and the masses of the various model components should therefore be approximately 1/216 of the masses of the equivalent prototype components. Prototype drop hammers typically have a mass of about 3000 kg which implies a model hammer mass of about 14 kg. The mass of a typical prototype drive mandrel and shoe, with a length to diameter ratio of 20, is about 1200 kg. The model mandrel and shoe therefore require a combined mass of about 5,5 kg. In the model tests the drop hammer had a mass of 16,5 kg and the mass of the model mandrel and pile shoe totalled 4,5 kg.

A parametric study on the effect of varying selected pile dimensions was carried out using the wave equation. It was found that the toe displacement per blow of the hammer (set), was particularly sensitive to hammer mass, hammer drop height and the pile toe resistance. The wave equation analysis predicted, however, that the selected model dimensions would produce toe displacements and shaft stresses which were of an acceptable order of magnitude.

B.1.2 Static Analysis

If it is assumed that for a given soil, the unit weight of that soil governs the soil strength properties relevant to pile capacity in a linear manner, then the basic variables required in a dimensional analysis can be listed as follows:

Load applied to the pile	Q	MLT^{-2}
Pile settlement under load	ρ	L
Pile radius	r	L
Elastic modulus of pile shaft	Ec	$ML^{-1}T^{-2}$
Pile length	L	L
Poissons ratio of soil	ν	1
Shear modulus of soil	G	$ML^{-1}T^{-2}$
Unit weight of soil	γ	$ML^{-2}T^{-2}$
Angle of internal friction of soil	ϕ	1

The settlement of the pile can be expressed as a function of the other variables,

$$\rho = f1\,(Q,\ r,\ E,\ L,\ \mu,\ G,\ \gamma,\ \phi) \qquad \ldots.\ (1)$$

If it is assumed that in the same soil μ and ϕ will be the same for both prototype and model, this equation reduces to,

$$\rho = f2\,(Q,\ r,\ E,\ L,\ G,\ \gamma) \qquad \ldots.\ (2)$$

Using r to eliminate L, and G to eliminate MT^{-2}, the following dimensionless groups are obtained,

$$\frac{\rho}{r} = f3\left(\frac{Q}{Gr^2},\ \frac{E}{G},\ \frac{L}{r},\ \frac{\gamma r}{G}\right) \qquad \ldots.\ (3)$$

Assuming pile settlement is proportional to the applied load, terms containing L and Q can be collected.

$$\frac{\rho G r^2}{rQ} = f4\left(\frac{E}{G}, \frac{L}{r}, \frac{\gamma r}{G}\right)$$

or

$$\rho = \frac{Q}{Gr} f4\left(\frac{E}{G}, \frac{L}{r}, \frac{\gamma r}{G}\right) \qquad \text{(B-4)}$$

Following Langhaar (1951, p.66) the following relationships can be developed (where K is the scale factor expressed as model dimension/prototype dimension),

$$K\rho = KQ \, . \, KG^{-1} \, . \, Kr^{-1} \qquad \text{(B-5)}$$

$$KE = KG \qquad \text{(B-6)}$$

$$KL = Kr \qquad \text{(B-7)}$$

$$KG = K\gamma Kr \qquad \text{(B-8)}$$

If it is accepted that for the model pile,

$$KE = KG = 1$$

then equation 8 becomes,

$$1 = K_\gamma \cdot Kr$$

and therefore,

$$K_\gamma = Kr^{-1} = KL^{-1} \qquad \text{(B-9)}$$

Substituting equation 8 into equation 5 yields the expression,

$$K_\rho = KQ \cdot K\gamma^{-1} \cdot Kr^{-2}$$

which using equations 7 and [illegible] can be simplified to,

$$K_\rho = KQ \cdot KL^{-1} \qquad \text{(B-10)}$$

On expansion this becomes,

$$\frac{\rho m}{\rho p} = \frac{\text{[illegible]}}{Qp} \cdot \frac{Lp}{Lm} \qquad \text{(B-11)}$$

where the subscripts m and p refer to model and prototype respectively. Equation 11 can be re-written as,

$$\frac{Qm}{\rho m} = \frac{Qp}{\rho p} \cdot \frac{Lm}{Lp} \qquad (B-12)$$

The following conclusions can be drawn from this analysis,

a) Equation 7 indicates that geometrical similitude is required in the model.

b) In order to model pile bearing capacity correctly, the soil unit weight should be scaled in inverse proportion to the linear scale (equation 9).

c) The load/settlement ratio of the model will be linearly related to the load/settlement ratio of the prototype.

APPENDIX C

Typical Computer Printout of Wave Equation Analyses

* PROGRAMME WAVE 4 *

****

PAGE NUMBER 1

****

NAME of CONTRACT:	MV Model Pile	JOB NUMBER	:1
RUN CODE	: 1		
RUN DATE	:	RUN PREPARED BY: JEG	

****

INPUT DATA

****

UNITS :- Typically kg mm seconds

Item 1. Number of mass elements ----------	= 5	No
Item 2. Mass of hammer -------------------	= 16.5	kg
Item 3. Mass of helmet -------------------	= .5	kg
Item 4. Mass/unit length of pile ---------	= .000865	kg/mm
Item 5. Elastic modulus of pile concrete	= 200	kN/mm^2
Item 6. Spring stiffness of dolly --------	= 5.65	kN/mm
Item 7. Spring stiffness of cushion ------	= 1[illegible]000	kN/mm
Item 8. Co-eff of restitution dolly ------	= .25	
Item 9. Co-eff of restitution cushion ---	= .55	
Item 10. Soil quake(under pile toe) ------	= 1	mm
Item 11. Damping co-effs: side and point	= .1 AND .23	ms/mm
Item 12. Pile C/S area -------------------	= 130	mm^2
Item 13. Pile element lengths ------------	= 400	mm
Item 14. Hammer drop hieght, and effiency	= 130 and .75	mm
Item 15. Time interval of calculation ----	= .05	ms
Item 16. Acceleration due to gravity -----	= .00981	mm/ms^2

	Total Static Ult Resistance	Percentage on Tip	Tip Resistance	Total Side Resistance
Case 1	1.306	87	1.13622	.16978
Case 2	2.612	93.5	2.44222	.16978

Side Resistances on each Element

Element Number	Case 1	Case 2
3	0.000	0.000
4	.060	.060
5	.110	.110

****

RESULTS

****

	Total Static Ult Resistance	Permanent Set
Case 1	1.306	7.76398771058
Case 2	2.612	3.57055610801

Maximum Compressive Forces

Distance From top	Case 1	Case 2
200	6.406	6.331
600	2.928	4.525
1000	2.665	4.164

Maximum Tensile Forces

Distance From top	Case 1	Case 2
200	0.000	0.000
600	.529	.373
1000	.533	.357

****

APPENDIX D

Calculation of Soil Strains

Soil strains were calculated from the sand grain displacement data obtained during both pile installation and static load testing, by applying the displacement method of analysis suggested by Clough (1965) and discussed by Smith (1971).

Consider the soil element shown with respect to a local co-ordinate system in Figure D.1. If u_n and v_n are assumed to vary linearly in the x and y directions given, then u_n and v_n are functions of x_n and y_n, and can be expressed in terms of displacement functions of the form:

$$u_n = \alpha_1 + x_n \alpha_2 + y_n \alpha_3 + x_n y_n \alpha_4 \quad \text{(D-1)}$$

$$v_n = \alpha_5 + x_n \alpha_6 + y_n \alpha_7 + x_n y_n \alpha_8 \quad \text{(D-2)}$$

Smith (1971, p.140) calls $\alpha_1, \alpha_2, \ldots \alpha_8$, the generalised co-ordinate displacement components.

In matrix form, these equations can be written as:

[Displacement vector] = (Co-ordinate matrix) x [Alpha vector]. (D-3)

$$\begin{bmatrix} u_1 \\ \cdot \\ \cdot \\ \cdot \\ v_4 \end{bmatrix} = \begin{bmatrix} 1 & x_1 & y_1 & x_1y_1 & 0 & 0 & 0 & 0 \\ \cdot & & & & & & & \\ \cdot & & & & & & & \\ \cdot & & & & & & & \\ 0 & 0 & 0 & 0 & 1 & x_4 & y_4 & x_4y_4 \end{bmatrix} \times \begin{bmatrix} \alpha_1 \\ \cdot \\ \cdot \\ \cdot \\ \alpha_8 \end{bmatrix} \quad \text{(D.4)}$$

According to Smith (1971 p.194), for the axially symmetric situation represented by the model pile, the radial strain components can be determined from the following relationships:

$$x = \frac{\partial u}{\partial v} \qquad \text{radial strain (X direction)}$$

$$y = \frac{\partial v}{\partial y} \qquad \text{vertical strain (Y direction)}$$

$$\varepsilon\theta = \frac{\partial u}{\partial x} \qquad \text{tangential strain} \qquad \text{(D-5)}$$

$$\gamma xy = \frac{\partial u}{\partial y} + \frac{\partial v}{\partial x} \qquad \text{shear strain (in X, Y plane)}$$

Differentiating the displacement functions matrix accordingly, we obtain the following relationship from which the radial strain components may be determined at each node of an element.

$$\begin{bmatrix} \varepsilon x_n \\ \varepsilon y_n \\ \varepsilon\theta_n \\ \gamma x_n y_n \end{bmatrix} = \begin{bmatrix} 0 & 1 & 0 & y_n & 0 & 0 & 0 & 0 \\ 0 & 0 & 0 & 0 & 0 & 0 & 1 & x_n \\ 1/x_n & 1 & y/x_n & y_n & 0 & 0 & 0 & 0 \\ 0 & 0 & 1 & x_n & 0 & 1 & 0 & y_n \end{bmatrix} \times \begin{bmatrix} \alpha_1 \\ \cdot \\ \cdot \\ \cdot \\ \cdot \\ \cdot \\ \alpha_8 \end{bmatrix} \quad \text{(D.6)}$$

Having determined the radial strain components, the principal strain components and their directions, and the maximum shear strains can be obtained by application of a Mohr strain circle. Volumetric strains may be obtained by summing the radial, vertical and tangential strains. This expression for volumetric strain is acceptably accurate for radial, vertical and tangential strain components up to strain magnitudes of the order of 10%. Above this strain level, second order terms in the full expression for volumetric strain become significant. Although the volumetric strain data was generated using the simpler three term expression, it is estimated that errors in the calculated strain data used to generate the volumetric strain diagrams does not exceed 3%. Only figure 6.19 has been affected by this error. The affected areas in this diagram are small and isolated and restricted to zones near both the point and base of the shoe cone.

The rectangular grid systems shown in Figures 6.7 and 6.20 were used with a computer program to calculate, using the abovementioned technique, the soil strains which occurred during both pile installation and static loading respectively. For the purpose of this analysis, the grids were treated as if the nodes lying along the edge of the pile were located within the soil boundary layer. The grids therefore refer to movements occurring only within the soil fabric. Sand grain displacement